PERGAMON

International Journal of Heat and Mass Transfer 45 (2002) 25–35

International Journal of HEAT and MASS TRANSFER

www.elsevier.com/locate/ijhmt

Thermally developing flow in elliptic ducts with axially variable wall temperature distribution

V.D. Sakalis [a,*], P.M. Hatzikonstantinou [a], N. Kafousias [b]

[a] *Department of Engineering Science, University of Patras, GR 26500 Patras, Greece*
[b] *Department of Mathematics, University of Patras, GR 26500 Patras, Greece*

Received 28 June 2000; received in revised form 6 April 2001

Abstract

The laminar, incompressible, hydrodynamically fully developed and thermally developed and developing flow is studied in straight elliptic ducts with aspect ratio a^* varying from 0.25 to 0.99 (which is an almost circular duct). The duct wall is subjected successively to constant temperature, to circumferential uniform and axially linearly or exponentially varying temperature. Numerical results obtained with the ADI scheme indicate that the friction factor increases as aspect ratio a^* decreases. In the thermally developing flow a high Nusselt number decreases as a^* decreases. In the thermally developed limit as a^* decreases, the Nusselt number increases for small axial wall temperature distributions, while decreases for large axial wall temperature values.

1. Introduction

The use of ducts with elliptic cross-section increases in the modern engineering heat transfer applications such as compact heat exchangers, flow passages, etc. The main advantage of using elliptic ducts than circular ducts is the increase of heat transfer coefficient. On the other hand, for the improvement of the performance of these exchangers, the accurate study of the thermally developing flow near the entrance region is essential.

The problem of flow into straight ducts of elliptic cross-section has received much attention during the past years, either for hydrodynamically developing-developed flow or thermally developing-developed heat transfer, in a wide range of thermal boundary conditions of the form $T_w = \text{constant}$ (constant wall temperature circumferentially and axially) or of the form $H1$ (axial uniform wall heat flux with peripherally uniform wall temperature), etc.

Many experimental, analytical and numerical procedures have been proposed in the literature (for a brief description [1,2]).

For the procedures using numerical methods (such as finite differences, finite volumes and finite elements), the discretization of the elliptical computational domain has been made adopting a rectangular grid [3] or developing a numerical generated boundary fitted coordinate [4]. On the other hand, an elliptical–cylindrical coordinate system has been used recently by Velusamy and Garg [5], for the study of hydrodynamically developed and thermally developing flow with thermal boundary conditions T_w and $H1$ for ducts of semi-elliptic cross-section, as well as in [6], for the study of the same problem in vertical elliptic ducts including buoyancy forces and $H1$ thermal boundary condition. A similar coordinate system has been used by Saatjian et al. [7] for the study of the flow between porous confocal elliptic duct and by Velusamy and Garg [8,9], for the study of the hydrodynamically developing flow without thermal effects. For all the above numerical procedures (and also for experimental and analytical), the wall temperature has been considered as constant in the axial direction of the straight pipe.

Javeri [10], using a variational Galerkin–Kantorowich method, analyzes the hydrodynamically developed and thermally developing flow and heat transfer, into straight ducts of square, circular and elliptic cross-section, for the thermal boundary condition of linearly

* Corresponding author.
E-mail address: vsakalis@hotmail.com (V.D. Sakalis).

0017-9310/02/$ - see front matter
PII: S0017-9310(01)00124-7

Nomenclature

A	source term in Eqs. (7a)–(7c)
B	axial conduction term in Eqs. (7a)–(7c)
a	semi-major axis
a^*	aspect ratio of the elliptic duct axis ($= b/a$)
b	semi-minor axis of the elliptic cross-section
c	eccentricity (nondimensional) ($= (1 - a^{*2})^{1/2}$)
C_1	coefficient in the LAWT case, with dimensions of [T][L^{-1}]
C_2'	coefficient in the EAWT case, with dimensions of [L^{-1}]
C_2	dimensionless coefficient in Eq. (7c) ($= aRePrC_2'$)
C_3	coefficient in the EAWT case, with dimensions of [T]
C_p	heat capacity of the fluid
D_h	hydraulic diameter of the elliptic cross-section, Eq. (6)
E	cross-section area
f	friction number
H_s	($= \sinh^2 \xi + \sin^2 n$)
k	heat conduction coefficient of the fluid
L_{th}	thermal entrance length
[L^{-1}]	dimensions of inverse distance
n	component of elliptic-orthogonal coordinate system, Fig. 1
$n_0,\ n_1$	minimum and maximum values of coordinate n ($n_0 = 0, n_1 = \pi/2$)
Nu	local Nusselt number, Eqs. (11) and (14)
$\overline{Nu_1}$	mean Nusselt number, Eq. (15)
$\overline{Nu_2}$	mean Nusselt number defined from energy balance, Eq. (16)
P	pressure (dimensionfull)
Pe	Peclet number ($= RePr$)
Pr	Prandtl number ($= \mu C_p/k$)
Re	Reynolds number ($= \rho w_m D_h/\mu$)
s	axial coordinate (dimensionfull)
$\overline{s}$	axial coordinate, dimensionless ($= s/(aRePr)$)
T	dimensionfull temperature
$\overline{T}$	dimensionless temperature of the fluid ($= (T - T_0)/(T_w - T_0)$)
T_w	temperature of the duct wall (dimensionfull)
$\overline{T_w}$	dimensionless temperature of the duct wall ($= 1$)
T_0	temperature of the duct inlet (dimensionfull)
$\overline{T_0}$	dimensionless temperature of the duct inlet ($= 0$)
$\overline{T_m}$	dimensionless bulk (mean) fluid temperature, Eq. (13)
[T]	dimensions of temperature T
t'	dimensionfull time
t	dimensionless time ($= t'\mu/(\rho a^2)$)
w	axial velocity (dimensionfull)
$\overline{w}$	dimensionless axial velocity ($= -\mu w/(a^2(dP/ds))$)
w_m	mean axial velocity (dimensionfull)
$\overline{w_m}$	dimensionless mean axial velocity, Eq. (5)
y_b	dimensionless distance measured along the semi-minor axis from the center of the ellipse to the wall

Greek symbols

ε	parameter in Eq. (17)
μ	viscosity of the fluid
ξ	component of the elliptic coordinate system, Fig. 1
$\xi_0,\ \xi_1$	minimum and maximum values of coordinate ξ ($\xi_0 = 0, \xi_1 = \tanh^{-1}(b/a)$)
Π	perimeter of the ellipse
ρ	density of the fluid

Subscripts

w	value at the wall
m	mean value

varying wall temperature in the axial direction (LAWT). Also, Abdel-Wahed et al. [11] have investigated experimentally the simultaneously developing hydrodynamic and thermal flow in straight elliptic ducts of aspect ratio 0.5 with the boundary condition of LAWT. Recently, the effect of the last boundary condition has been also investigated numerically by Rindt et al. [12] for the case of a curved duct with circular cross-section.

The present paper analyzes the problem of laminar, incompressible, hydrodynamically fully developed and thermally developing flow into straight ducts of elliptic cross-section with various aspect ratios $b/a = 0.8$, 0.5, 0.25, including the nearly circular cross-section with $b/a = 0.99 \cong 1$. Numerical results are obtained for the investigation of the flow and heat transfer characteristics using an applicable elliptical–cylindrical coordinate system for the exact application of the boundary condition at the wall. Accordingly, the equations of momentum, energy and other parameters of the problem (Nu, fRe, etc.) are formulated in the adopted coordinate system. The duct wall is subjected successively to the following three thermal boundary conditions: peripherally constant as well as linearly and exponentially varying wall temperature in the axial direction, denoted as LAWT and EAWT, respectively. Interesting results for all cases are presented while the EAWT boundary condition is investigated for the first time. The chosen boundary conditions are applied in counter flow heat exchangers and solar domestic heat water systems. Linear and weekly nonlinear axial wall temperature

variations are observed in various situations of the above systems.

The effect of axial conduction is neglected considering thermal flow with large Peclet number. The effect of buoyancy forces is also neglected because we consider small temperature differences between the wall and the core region of a fluid having large Reynolds number. Fluid properties assume to be constant and independent of temperature.

2. Analysis

We consider the laminar flow of incompressible fluid entering a straight duct of elliptical cross-section. Assuming negligible body forces we consider a hydrodynamically fully developed and thermally developing flow neglecting the momentum diffusion in the axial direction. For the study of flow and heat transfer characteristics, we consider the elliptical orthogonal coordinate system (s, ξ, n), shown in Fig. 1.The component s is the axial coordinate and ξ, n are the coordinates in the plane of the cross-section. The surfaces $\xi =$ constant are the confocal elliptic cylinders

$$\frac{x^2}{(\cos n)^2} - \frac{y^2}{(\sin n)^2} = 1 \tag{1}$$

while the surfaces $n =$ constant are the hyperbolic cylinders

$$\frac{x^2}{(\cosh \xi)^2} + \frac{y^2}{(\sinh \xi)^2} = 1. \tag{2}$$

The nondimensionalized equations of motion and energy, transformed into the above coordinate systems can be expressed as:

Axial momentum equation

$$c^2 H_s \frac{\partial \overline{w}}{\partial t} = \frac{\partial^2 \overline{w}}{\partial \xi^2} + \frac{\partial^2 \overline{w}}{\partial n^2} + c^2 H_s. \tag{3}$$

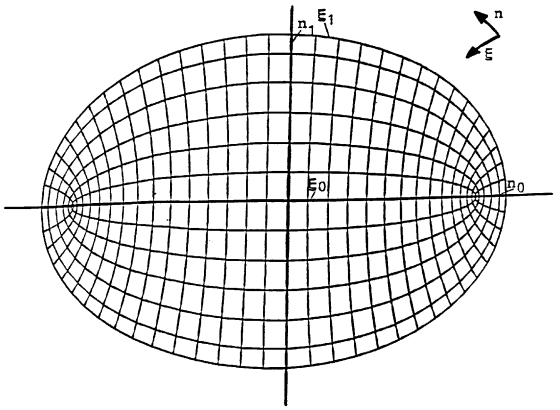

Fig. 1. Elliptical–cylindrical coordinate system.

Energy equation

$$c^2 H_s \frac{\overline{w}}{\overline{w}_m} \left(\frac{a}{D_h}\right) \left(\frac{\partial \overline{T}}{\partial \bar{s}} + A\right) = \frac{\partial^2 \overline{T}}{\partial \xi^2} + \frac{\partial^2 \overline{T}}{\partial n^2} + B, \tag{4}$$

where $\overline{T} = (T - T_0)/(T_w - T_0)$.

The mean axial velocity of the flow w_m is given by

$$\overline{w}_m = \frac{4(a^{*2} - 1)}{\pi a^*} \int_{n_0}^{n_1} \int_{\xi_0}^{\xi_1} \overline{w} H_s \, d\xi \, dn, \tag{5}$$

where c is the eccentricity of the elliptic cross-section, a^* is the aspect ratio of the elliptic duct axis, a the semi-major axis and D_h the hydraulic diameter

$$D_h = \frac{4\Pi}{E} = 2\pi \left(\frac{1}{2}\left(a^2 + b^2\right)\right)^{1/2} \quad \text{and}$$
$$\left(\frac{D_h}{a}\right) = \frac{2a^*}{\sqrt{\frac{1}{2}(1 + a^{*2})}}. \tag{6}$$

The terms A and B depend on the imposed thermal boundary conditions.

For the dimensional wall temperature boundary condition $T_w =$ constant

$$A = 0 \quad \text{and} \quad B = \frac{1}{(RePr)^2} \frac{\partial^2 \overline{T}}{\partial \bar{s}^2}. \tag{7a}$$

For the dimensional LAWT case with $T_w - T_0 = C_1 s$

$$A = \frac{\overline{T}}{\bar{s}} \quad \text{and} \quad B = \frac{1}{(RePr)^2} \left[\frac{\partial^2 \overline{T}}{\partial \bar{s}^2} + \frac{2}{\bar{s}} \frac{\partial \overline{T}}{\partial \bar{s}}\right]. \tag{7b}$$

For the dimensional EAWT case with $T_w - T_0 = C_3 \exp(C_2' s) = C_3 \exp(C_2 \bar{s})$

$$A = \overline{T} C_2 \quad \text{and}$$
$$B = \frac{1}{(RePr)^2} \left[\frac{\partial^2 \overline{T}}{\partial \bar{s}^2} + 2C_2 \frac{\partial \overline{T}}{\partial \bar{s}} + C_2^2 \overline{T}\right], \tag{7c}$$

where $C_2 = aRePrC_2'$.

The constants C_1, C_2', and C_3 have dimensions of [T][L^{-1}], [L^{-1}] and [T], respectively. However the constants C_1 and C_3 do not appear in the final equations.

Numerical studies indicate that, for $T_w =$ constant and for values of the Peclet number $Pe > 50$ [1], the term B, representing the thermal axial conduction, via the relation (7a), can be neglected. Similar results apply for the LAWT case where B is given by (7a). In the EAWT case, B can be neglected only if the coefficients $(RePr)^{-2}$, $2C_2(RePr)^{-2}$ and $C_2^2(RePr)^{-2}$ are of the same neglected magnitude. The term B can be neglected for $Pe > 50$ when $C_2 = 1$, $Pe > 500$ when $C_2 = 10$ and $Pe > 5000$ when $C_2 = 100$.

It is observed that the application of the nonlinear EAWT boundary condition reveals the conditions under which the effects of the axial conduction may be neglected.

In the present study the thermal axial conduction is neglected for all cases.

The imposed dimensional velocity and thermal boundary conditions are expressed in the following nondimensional form:

$$\overline{w} = 0 \text{ along } \xi = \xi_0 = \tanh^{-1}(a^*) \quad \text{for all } n, \tag{8a}$$

$$\overline{T} = \overline{T}_0 = 0 \text{ at } \bar{s} = 0 \quad \text{for all } \xi \text{ and } n, \tag{8b}$$

$$\overline{T} = \overline{T}_w = 1 \text{ at } \xi = \xi_0 \quad \text{for all } n. \tag{8c}$$

Owing to the symmetry of the flow, only a quarter of the elliptic cross-section is used in the numerical procedure. Accordingly, the following symmetry boundary conditions are needed:

$$\frac{\partial \overline{w}}{\partial n} = \frac{\partial \overline{T}}{\partial n} = 0 \text{ along } \xi = \xi_1 = 0 \quad \text{for all } n, \tag{9a}$$

$$\frac{\partial \overline{w}}{\partial \xi} = \frac{\partial \overline{T}}{\partial \xi} = 0 \text{ along } n = n_0 = 0 \quad \text{for all } \xi, \tag{9b}$$

$$\frac{\partial \overline{w}}{\partial n} = \frac{\partial \overline{T}}{\partial n} = 0 \text{ along } n = n_1 = \frac{\pi}{2} \quad \text{for all } \xi. \tag{9c}$$

Physical quantities of primary interest are the local friction factor and the local Nusselt number, which are defined, respectively, by

$$f = \frac{-(\mathrm{d}P/\mathrm{d}s)D_h}{2\rho w_m^2}, \tag{10}$$

$$Nu = \frac{hD_h}{k}, \tag{11}$$

where h is the local heat transfer coefficient.

The characteristic quantity of fluid flow fRe expressed in terms of hydraulic diameter and nondimensional quantities takes the form

$$fRe = \left(\frac{D_h}{a}\right)^2 \frac{1}{2\overline{w}_m}, \tag{12}$$

where Re is the Reynolds number.

Considering the bulk (mean) fluid temperature of flow which is given by

$$\overline{T}_m = \frac{\int_{n_0}^{n_1} \int_{\xi_0}^{\xi_1} \overline{w}\overline{T} H_s \,\mathrm{d}\xi \,\mathrm{d}n}{\int_{n_0}^{n_1} \int_{\xi_0}^{\xi_1} \overline{w} H_s \,\mathrm{d}\xi \,\mathrm{d}n} \tag{13}$$

the local Nusselt number Nu and the mean local $\overline{Nu_1}$ are given by the expressions:

$$Nu = \left(\frac{1}{1-\overline{T}_m}\right)\left(\frac{D_h}{a}\right)\left(H_s^{1/2}\frac{\partial \overline{T}}{\partial \xi}\right)\Big|_{\xi=\xi_1}, \tag{14}$$

$$\overline{Nu_1} = \frac{\int_{n_0}^{n_1} Nu H_s \,\mathrm{d}n}{\int_{n_0}^{n_1} H_s \,\mathrm{d}n}. \tag{15}$$

Another expression for the mean Nusselt number can be obtained from the consideration of the energy balance over the entire cross-section and is given by the formula:

$$\overline{Nu_2} = -\frac{1}{4}\left(\frac{1}{1-\overline{T}_m}\right)\left(\frac{D_h}{a}\right)\frac{\mathrm{d}\overline{T}_m}{\mathrm{d}\bar{s}}. \tag{16}$$

3. Solution

The set of uncoupled Eqs. (3) and (4) for the cases (7a)–(7c) subjected to the boundary conditions (8a)–(8c) and (9a)–(9c) is solved numerically employing the iterative finite difference pseudotransient alternating direction implicit method (ADI). For the discretization of these equations, three-point central differences are used for the second-order derivatives and two-point forward differences for the first-order derivatives. So, an algebraic system of equations is obtained for each variable which is solved by the well-known tridiagonal matrix algorithm (TDMA).

Consequently, the friction factor product fRe and the local and mean Nusselt numbers are calculated using Eqs. (12), and (15), and (16), respectively.

Convergence of the iteration procedure for both the momentum and energy equations was achieved when the following criterion was satisfied:

$$\left(\frac{1}{N^2}\sum_{\xi=\xi_0}^{\xi_1}\sum_{n=n_0}^{n_1}\left|B(\xi,n)^{m+1} - B(\xi,n)^m\right|^2\right)^{1/2} \leqslant \varepsilon, \tag{17}$$

where $B(\xi, n)$ represents the variable $\overline{w}$ or $\overline{T}$, respectively, m is the iteration number, N is the total number of grid points and $\varepsilon = 10^{-6}$.

The integrals of mean velocity Eq. (5), bulk fluid temperature Eq. (13) and mean Nusselt numbers relations (15) and (16) are calculated employing the SIMPSON rule. Accurate results for the Eq. (14)–(16) are obtained using three-point forward differences for the first-order derivatives. Considering the symmetry of the flow, as we referred before, only a quarter of the whole cross-section was used in the numerical computation.

Uniform grid pattern of 40×40 points is employed for elliptic cross-sections with aspect ratios $a^* = 0.8$, 0.5 and 0.25. For the circular cross-section with $a^* = 0.99 \cong 1$, a 50×50 uniform grid pattern is used. All the successive calculations of the present paper are based on these grid sizes. To assure the accuracy of the numerical results, numerical tests have been made with different grids, in order to determine the effect of the grid size in the numerical results: so, for the cases of $a^* = 0.8$, 0.5 and 0.25 a uniform grid of 30×30 points, and for $a^* = 0.99 \cong 1$ a grid of 40×40 points, have been also used.

In Table 1 temperature and velocity results are presented along the minor axis for the case of $b/a = 0.25$, using a coarse (30×30) and a fine (40×40) grid. The mean deviations of the results obtained for the velocity and temperature with the two grids are about 0.20% and

Table 1
Temperature and velocity profiles as functions of the distance y_b, measured along the semi-minor axis from the center of the ellipse to the wall

Temperature $\overline{T}(y_b)$				Axial velocity $\overline{w}(y_b)$			
y_b	30×30 grid	40×40 grid	Deviation (%)	y_b	30×30 grid	40×40 grid	Deviation (%)
0	0.02409	0.02420	0.454	0	0.16293	0.15447	5.480
0.02473	0.02393	0.02402	0.376	0.02473	0.17184	0.16425	4.420
0.04948	0.02331	0.02338	0.300	0.04948	0.20162	0.19483	3.370
0.07426	0.02221	0.02227	0.270	0.07426	0.25289	0.24686	2.384
0.09909	0.02063	0.02068	0.242	0.09909	0.32417	0.31889	1.628
0.12399	0.01856	0.01859	0.161	0.12399	0.41307	0.40859	1.084
0.14896	0.01597	0.01599	0.125	0.14896	0.51638	0.51275	0.703
0.17404	0.01284	0.01286	0.155	0.17404	0.63034	0.62759	0.436
0.19922	0.00916	0.00917	0.109	0.19922	0.75103	0.74920	0.244
0.22454	0.00489	0.00489	0	0.22454	0.87504	0.87416	0.101
0.25	0	0	0	0.25	1	1	0

1.80%, respectively. Similar mean deviations are observed for the results obtained with the other aspect ratios. The mean deviation between coarse and fine grids for each case of aspect ratio is less than 0.5% for *fRe* and less than 1.9% for the Nusselt number.

The time step Δt in the momentum equation depends on the plane grid size (i.e., $\Delta\xi$, Δn steps) and gradually on the parameter c of the elliptic cross-section. Generally, Δt is between 10^{-4} and 1.8×10^{-5}. Especially, for $a^* = 0.99$, $\Delta t = 0.0001$ for $a^* = 0.8$, $\Delta t = 0.0002$ for $a^* = 0.5$, $\Delta t = 0.00005$ and for $a^* = 0.25$, $\Delta t = 0.000018$. Along the axial direction a fine grid of size $\Delta s = 10^{-6}$ was used near the duct entrance to avoid numerical fluctuations, especially for lower grid sizes. As the flow becomes gradually thermally fully developed, in quite a long axial position from the entrance of the duct, an axial step size Δs of about 10^{-4} is considered as satisfactory.

All the present results for the Nusselt number are based on Eq. (15). The maximum deviation of the Nusselt numbers given by Eqs. (15) and (16) is less than 2%. This fact ensures the accuracy of numerical results too.

As we stated before, the discretization of the second-order derivatives in momentum and energy equation is based on three-point finite differences. The use of higher-order discretization, such as five-point finite differences, leads to five-diagonal algebraic systems. Although five-point discretization is more accurate than that of three-points, the maximum difference in the results of friction factor and Nusselt number for the two cases was found to be less than 1%. Consequently, there is no reason to use five-point instead of three-point discretization in the second-order derivatives.

4. Accuracy

In order to validate the accuracy of the numerical results, we have performed computations on the well-studied problem of thermally developed flow in straight elliptic duct with constant wall temperature $T_w =$ constant. The obtained results for the friction factor and the Nusselt number for the values of aspect ratio $a^* = 0.99$, 0.8, 0.5 and 0.25 are shown in Table 2 along with the analytical results of Schenk and Han [13]. Comparison of the results of Table 2 indicates very close agreement. The maximum deviation is less than 0.434% for *fRe* and less than 1.871% for Nusselt number, while the mean deviation is 0.28% and 0.69%, respectively. It is observed that as α^* decreases the increase of $\overline{Nu_1}$ is very small.

For the thermally developing flow, the development of the Nusselt number, as a function of the axial distance $\bar{s}$ from the entrance of the duct, under the thermal boundary conditions $T_w =$ constant and LAWT, is shown in Tables 3 and 4, respectively. In Table 3 the analytical results of [14] are also presented. It is observed

Table 2
Mean Nusselt number $\overline{Nu}_1$ and friction factor product *fRe* for thermally developed flow with $T_w =$ constant

$a^* = b/a$	$\overline{Nu}_1$ (present)	*Nu* [13]	Deviation *Nu* (%)	*fRe* (present)	*fRe* [13]	Deviation *fRe* (%)
1	3.655	3.658	0.082	16.02	16.0	0.125
0.8	3.694	3.669	0.681	16.255	16.317	0.380
0.5	3.672	3.742	1.871	16.896	16.823	0.434
0.25	3.692	3.687	0.136	18.258	18.29	0.175

Table 3
Mean Nusselt number $\overline{Nu}_1$ for thermally developing flow in circular duct ($b/a = 0.99$) with $T_w = \text{constant}$

$\bar{s}$	Nu (analytical) [14]	$\overline{Nu}_1$ (present)	Difference (%)
0.001	12.80	13.3686	4.44
0.004	8.03	8.09398	0.796
0.01	6.00	6.00197	0.033
0.04	4.17	4.1629	0.17
0.08	3.77	3.7647	0.14
0.1	3.71	3.7078	0.06
0.2	3.66	3.6577	0.063
∞	3.66	3.6577	0.063

that the deviation of the results for $\bar{s} = 0.001$ is 4.44% and the mean deviation for $\bar{s} > 0.001$ is about 0.19%. This is due mainly to the large axial and transverse temperature gradients in the vicinity of the entrance of the flow. It is verified by the fact that for $\bar{s} = 0.001$ the deviation of the $\overline{Nu}_1$ decreases for a finer grid of 80×80 to 2.3%, while it increases for a coarse grid of 40×40 to 5.46%. Similar behavior of the numerical results is presented in the relevant work of [15].

Similar results are presented in Table 4 for the aspect ratio numbers $a^* = 0.99$, 0.8, 0.5, 0.25. The results obtained by Javeri [10] using the Kantoriwich variational method are presented also in Table 4 only for the case of circular duct. His results for elliptic ducts cannot be compared with ours because of the different nondimensional variables used. Comparing our results with those of Javeri [10] for the circular duct, we observe a maximum deviation of about 36% in the position $\bar{s} = 0.01$. This deviation decreases as the distance s increases and becomes 0.3% at $\bar{s} = 1$. Considering the very good agreement of our results with those of Schenk et al. [13] and Kays and Crawford [14] presented in Tables 2 and 3, we conclude that the deviation of Javeri's results is mainly due to the omission of higher order terms in his approximate solutions. Recently, in the thermally developing region, similar in order of magnitude differences have been observed by Abdel-Wahed [11], where experimentally investigated the problem of simultaneously hydrodynamical and thermally developing flow in an elliptic duct of aspect ratio 0.5, when the wall is subjected to LAWT boundary condition. Unfortunately, their results cannot be compared absolutely with ours, owing to different hydrodynamic flow considerations.

5. Results and discussion

Fig. 2 represents the variation of the axial velocity w along the semi-minor axis of the elliptic duct for various aspect ratios. For all aspect ratios, the parabolic character of the axial velocity is obvious.

Table 4
Mean Nusselt number $\overline{Nu}_1$ for thermally developing flow with $T_w - T_0 = C_1 s$

$\bar{s}$	$\overline{Nu}\ b/a = 1$ [10]	$\overline{Nu}_1\ b/a = 1$ (present)	Deviation (%)	$Nu\ b/a = 0.5$ [10]	$\overline{Nu}_1\ b/a = 0.5$ (present)	Deviation (%)	$Nu\ b/a = 0.25$ [10]	$\overline{Nu}_1\ b/a = 0.25$ (present)	Deviation (%)	$\overline{Nu}_1\ b/a = 0.8$ (present)
0.001	22.847	21.682	5.1	24.325	17.441	–	26.402	14.466	–	19.874
0.002	21.579	16.709	22.6	23.450	13.754	–	25.482	11.515	–	15.506
0.005	18.419	11.959	35.1	20.954	10.153	–	22.860	8.651	–	11.295
0.01	14.748	9.405	36.2	17.749	8.170	–	19.502	7.110	–	8.989
0.02	10.763	7.518	30.1	13.814	6.695	–	15.395	6.02	–	7.257
0.05	7.093	5.813	18.0	9.113	5.404	–	10.469	5.153	–	5.701
0.1	5.682	5.026	11.5	6.921	4.857	–	8.018	4.830	–	4.998
0.2	4.925	4.602	6.6	5.682	4.595	–	6.470	4.714	–	44.633
0.5	4.482	4.411	1.58	4.888	4.514	–	5.402	4.699	–	4.483
1	4.380	4.3938	0.23	4.641	4.511	–	5.041	4.699	–	4.473
∞	4.364	4.3934	0.6	4.558	4.511	1.03	4.880	4.699	3.7	4.473

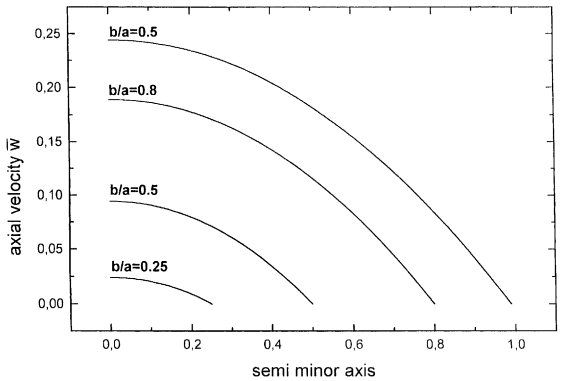

Fig. 2. The axial velocity $\overline{w}$ along the semi-minor axis of the elliptic duct for various aspect ratios.

The results for the friction factor in the hydrodynamically fully developed flow through elliptical ducts with various aspect ratios are presented in Table 2. It is observed that, as the aspect ratio varies from 1 to 0.25 the friction factor increases about 13.5%. However, we observe that in the case of fully developed thermal flow with $T_w = \text{constant}$ for $a^* = 0.5$, where the Nusselt number reaches its maximum increase, about 2.3%, the increase of the friction factor is restricted to about 5.14%.

From Table 4, it is observed that in the limiting case of thermally fully developed flow ($\bar{s} \geqslant 1$), under the LAWT boundary condition, the mean Nusselt number $\overline{Nu_1}$ increases from 4.393 to 4.699, that is about 7%, as the aspect ratio decreases from 1 to 0.25. Similarly, from Table 5, it is observed that in the thermally fully developed flow ($\bar{s} \geqslant 1$), under the EAWT boundary condition with low values of C_2, the $\overline{Nu_1}$ increases as the aspect ratio decreases from 1 to 0.25. In the vicinity of the moderate value $C_2 = 10$ the $\overline{Nu_1}$ fluctuates. However, as C_2 increases to larger values, the above behavior of the Nusselt number is reversed and decreases as the aspect ratio decreases from 1 to 0.25 (this behavior is more obvious in Fig. 13).

Results for $\overline{Nu_1}$, in the thermally developing flow, are presented in Tables 3 and 4, for the boundary conditions $T_w = \text{constant}$ and LAWT, respectively. From Table 4, it is observed that near the entrance region, the decrease of the aspect ratio yields the decrease of the Nusselt number. Clearly, for the purpose of the heat transfer enhancement it is better to use ducts with low values of aspect ratio.

Tables 6 and 7 presents the thermal entrance length L_{th} for values of aspect ratio $a^* = 0.99$, 0.8, 0.5, 0.25 under the LAWT and EAWT thermal boundary conditions, respectively. The length L_{th} is the axial position where the local Nusselt number becomes 1.05 times the value of the Nusselt number (that is 5% larger) in the thermally fully developed flow [1]. For the case of

Table 5
Mean Nusselt number Nu_1 for thermally developing flow with $T_w - T_0 = C_3 \exp(C_2 s)$

$\bar{s}$	$\overline{Nu_1}$ $b/a = 1$			$\overline{Nu_1}$ $b/a = 0.8$			$\overline{Nu_1}$ $b/a = 0.5$			$\overline{Nu_1}$ $b/a = 0.25$		
	$C_2 = 1$	$C_2 = 10$	$C_2 = 100$	$C_2 = 1$	$C_2 = 10$	$C_2 = 100$	$C_2 = 1$	$C_2 = 10$	$C_2 = 100$	$C_2 = 1$	$C_2 = 10$	$C_2 = 100$
0.005	7.505	7.710	9.551	7.178	7.369	9.090	6.806	6.973	8.467	5.835	5.973	7.188
0.01	6.024	6.341	8.909	5.788	6.086	8.494	5.571	5.84	7.962	4.945	5.169	6.879
0.05	4.099	4.943	8.729	4.038	4.832	8.338	4.098	4.853	7.865	4.069	4.757	6.903
0.1	3.887	4.987	8.73	3.888	4.910	8.339	4.01	4.996	7.867	4.103	4.972	6.905
1	4.461	5.143	8.73	4.468	5.063	8.339	4.67	5.145	7.867	4.781	5.072	6.875
∞	4.461	5.143	8.73	4.468	5.063	8.339	4.67	5.145	7.867	4.781	5.072	6.875

Table 6
Thermal entrance length L_{th} with $T_w - T_0 = C_1 s$

L_{th} $b/a = 0.99$ (LAWT)	L_{th} $b/a = 0.8$ (LAWT)	L_{th} $b/a = 0.5$ (LAWT)	L_{th} $b/a = 0.25$ (LAWT)
0.1948	0.1684	0.1277	0.0752

Table 7
Thermal entrance length Lth with $T_w - T_0 = C_3 \exp(C_2' s)$

L_{th} $b/a = 1$ (EAWT)			L_{th} $b/a = 0.8$ (EAWT)			L_{th} $b/a = 0.5$ (EAWT)			L_{th} $b/a = 0.25$ (EAWT)		
$C_2 = 1$	$C_2 = 10$	$C_2 = 100$	$C_2 = 1$	$C_2 = 10$	$C_2 = 100$	$C_2 = 1$	$C_2 = 10$	$C_2 = 100$	$C_2 = 1$	$C_2 = 10$	$C_2 = 100$
0.0255	0.0215	0.0069	0.0219	0.0188	0.0068	0.0165	0.0146	0.0062	0.0093	0.0085	0.0046

LAWT boundary condition, it is observed that as the aspect ratio varies from 0.99 to 0.25, the thermal entrance length L_{th} decreases about 63%. In the case of EAWT, for any value of aspect ratio, the thermal entrance length L_{th} decreases as the parameter C_2 increases (for example, when $b/a = 0.5$ L_{th} decreases about 69% as C_2 varies from 1 to 100). However, the interval of this variation decreases as the aspect ratio decreases. For any value of C_2, the length L_{th} decreases as the aspect ratio decreases from 1 to 0.25.

The variations of $\overline{Nu_1}$, $\overline{T_m}$ and $\overline{T}$, in the case of LAWT boundary condition, are shown in Figs. 3–7. Fig. 3 shows that in the entrance region the increase of the aspect ratio leads to increase of $\overline{Nu_1}$. Fig. 4 shows that the mean temperature of the fluid tends to unity when the flow reaches the thermally fully developed flow. Also, as the ratio decreases, the bulk temperature tends more rapidly to unity following lower profiles. Comparing the results of Figs. 3 and 4 with the corresponding ones obtained by Shah and London [1], we conclude that the values of $\overline{Nu_1}$ for the thermally developed flow, under the LAWT and $H1$ boundary conditions, are exactly the same for each aspect ratio.

Results for $\overline{Nu_1}$ and $\overline{T_m}$, in the thermally developing flow, under the EAWT boundary condition, are presented in Table 5 and Figs. 8–13. Table 5 presents the

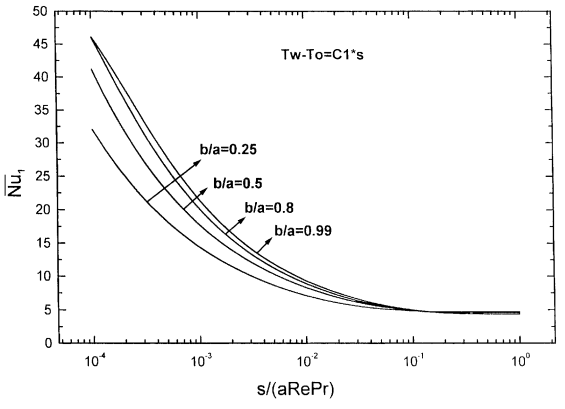

Fig. 3. The mean Nusselt number $\overline{Nu_1}(\bar{s})$ profiles for various values of $a^* = 0.99$, 0.8, 0.5, 0.25 in the LAWT case.

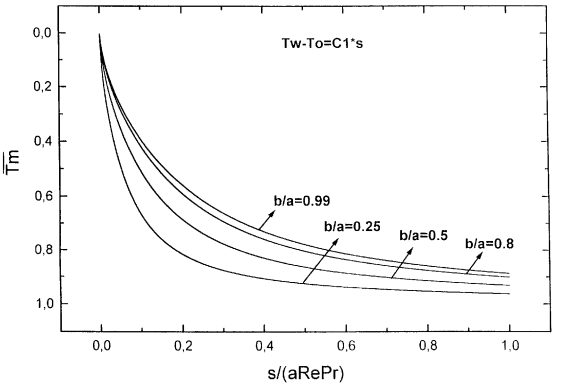

Fig. 4. The bulk fluid temperature $\overline{T_m}(\bar{s})$ profiles for various values of $a^* = 0.99$, 0.8, 0.5, 0.25 in the LAWT case.

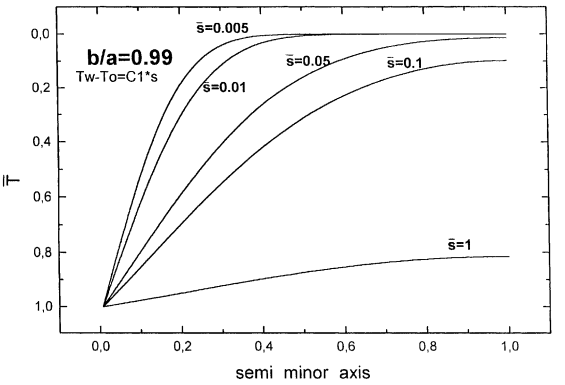

Fig. 5. Temperature distribution $\overline{T}$ along the semi-minor axis of the nearly circular duct ($a^* = 0.99$) for various values of the axial length $\bar{s}$ in the LAWT case.

mean Nusselt number as a function of $\bar{s}$, for the aspect ratios $a^* = 1$, 0.8, 0.5, 0.25 and the parametric values $C_2 = 1$, 10 and 100. The behavior of $\overline{Nu_1}$ is similar to that presented in Table 4.

Figs. 8 and 9 represent the variation of the mean Nusselt number against the axial position $\bar{s}$, for various aspect ratios with $C_2 = 1$ and $C_2 = 100$, respectively. In the entrance region the decrease of ratio a^* causes the

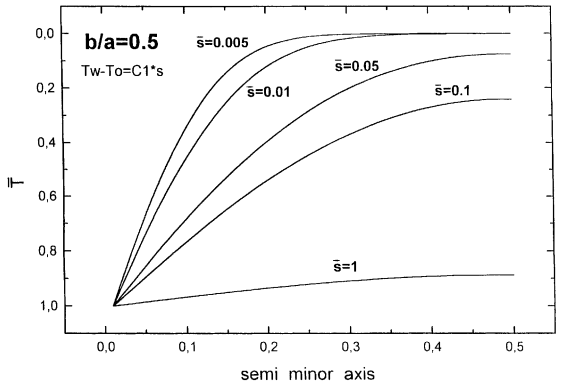

Fig. 6. Temperature distribution $\overline{T}$ along the semi-minor axis of elliptic duct with $a^* = 0.5$ for various values of the axial length $\bar{s}$ in the LAWT case.

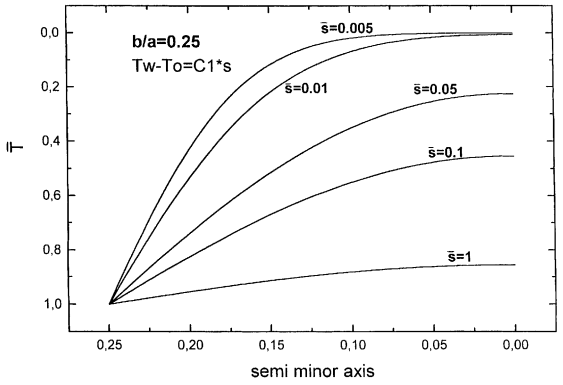

Fig. 7. Temperature distribution $\overline{T}$ along the semi-minor axis of elliptic duct with $a^* = 0.25$ for various values of the axial length $\bar{s}$ in the LAWT case.

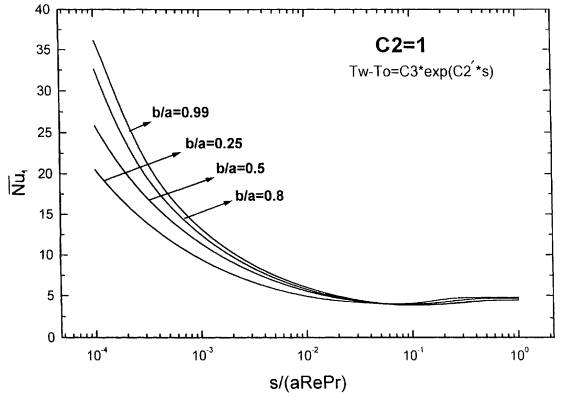

Fig. 8. The mean Nusselt number $\overline{Nu_1}(\bar{s})$ profiles for various values of a^* in the EAWT case with $C_2 = 1$.

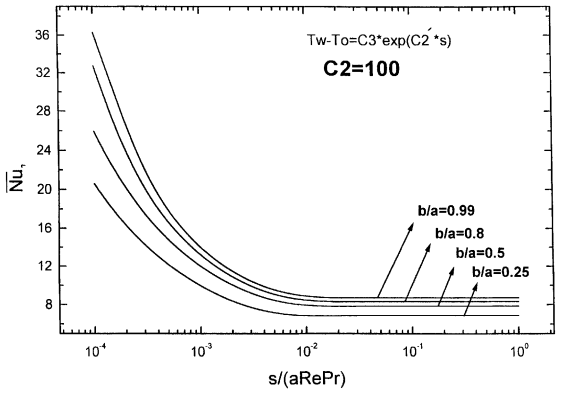

Fig. 9. The mean Nusselt number $\overline{Nu_1}(\bar{s})$ for various values of a^* with $C_2 = 100$ in the EAWT case.

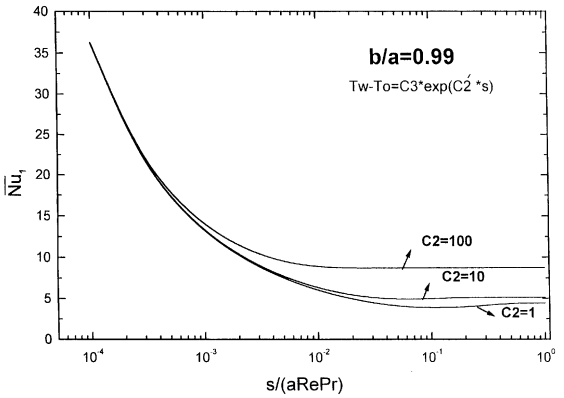

Fig. 10. The mean Nusselt number $\overline{Nu_1}(\bar{s})$ for various values of C_2 when $a^* = 0.99$ in the EAWT case.

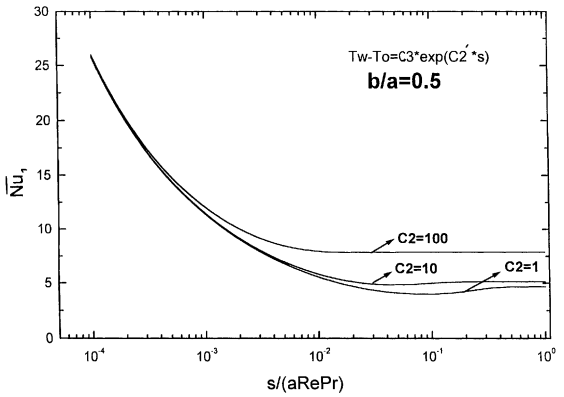

Fig. 11. The mean Nusselt number $\overline{Nu_1}(\bar{s})$ for various values of C_2 when $a^* = 0.5$ in the EAWT case.

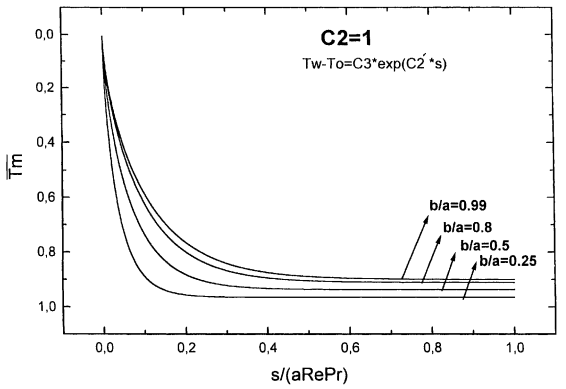

Fig. 12. The bulk fluid temperature $T_w(\bar{s})$ for various values of a in the EAWT case with $C_2 = 1$.

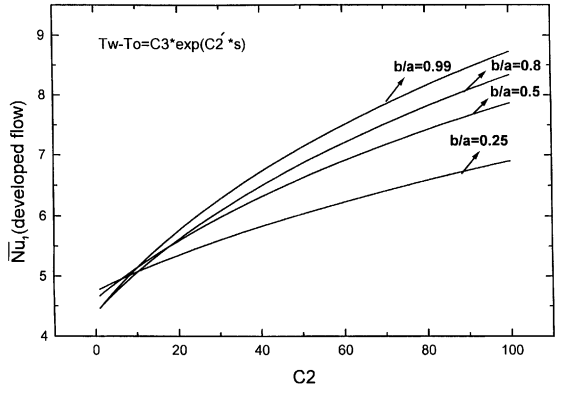

Fig. 13. The mean Nusselt number $\overline{Nu_1}$ in the thermal fully developed region, as a function of the parameter C_2 in the EAWT case, for various values of a^*.

decrease of Nusselt number. This behavior is reversed in the limit of fully developed thermal flow, for the cases of small values of C_2. In the thermally developed flow, for moderate values of $C_2 \cong 10$, the Nusselt number is almost constant for the various aspect ratios, while for large values of C_2 (see Fig. 13) the Nusselt number decreases.

Figs. 10 and 11 show the variation of Nusselt number against the axial position $\bar{s}$ for the values of $C_2 = 1$, 10, 100 and aspect ratios 0.99 and 0.5, respectively. For any given value of b/a, the increase of C_2 causes the increase of Nusselt number, both in the entrance and the developed region. Also, for low values of C_2, a 'concave' appears in the low part of the Nusselt number profile, which is mainly due to a slight inversion of the behavior of $\partial\overline{T}/\partial\bar{s}$.

The behavior of $\overline{T_m}$ as a function of $\bar{s}$ is shown in Fig. 12. Comparing these results with those of Fig. 4, we observe that $\overline{T_m}$ varies more sharply to its limiting values in the region $\bar{s} \leqslant 0.2$ in the EAWT case than the corresponding one of LAWT. In both cases $\overline{T_m}$ increases as a^* increases.

Finally, Fig. 13 shows the variation of $\overline{Nu_1}$ in the thermally developed region under the EAWT condition, as a function of the strength parameter C_2 for various values of the ratio a^*. As the aspect ratio decreases, $\overline{Nu_1}$ increases as C_2 decreases from $C_2 = 7$ to lower values and decreases as C_2 increases from $C_2 \cong 10$ to larger values.

6. Concluding remarks

As the aspect ratio of the elliptic duct a^* decreases from 0.99 to 0.25, the friction factor product fRe increases. For the boundary condition $T_w = \text{constant}$, as the aspect ratio decreases from 0.99 to about 0.5 the Nusselt number increases and from $a^* \cong 0.5$ to 0.25 the Nusselt number decreases.

For the case of LAWT and in the region of fully developed thermal flow, as the aspect ratio decreases from 0.99 to 0.25 the Nusselt number increases at about 7%. In the entrance region, the decrease of aspect ratio yields the decrease of Nusselt number.

In this case the thermal entrance length L_{th} decreases at about 63% as a^* varies from 0.99 to 0.25.

From the results of the EAWT condition, it is concluded that as the aspect ratio decreases, the Nusselt number for small and moderate values of $T_w - T_0$ increases, while for large values it decreases. Also, for any value of C_2, the thermal entrance length L_{th} decreases as aspect ratio varies from 0.99 to 0.25.

References

[1] R.K. Shah, A.L. London, Laminar Flow Forced Convection in Ducts, Academic Press, New York 1978 (Chapter IX, pp. 247–252, Chapter II, p. 7).
[2] S. Kakac, R.K. Shah, W. Aung, Handbook of Single Phase Convective Heat and Mass Transfer, Wiley, New York, 1988, pp. 63–68 (Chapter 3).
[3] M. Mahadevapa, V.R. Rao, M.K. Sastri, Numerical study of steady laminar fully developed fluid flow and heat transfer in rectangular and elliptical ducts rotating about a parallel axis, Int. J. Heat Mass Transfer 39 (4) (1996) 867–875.
[4] Z.F. Dong, M.A. Ebadian, A numerical analysis of thermally developing flow in elliptic ducts with internal fins, Int. J. Heat Fluid Flow 12 (2) (1991) 166–172.
[5] K. Velusamy, V.K. Garg, G. Vaidyanathan, Fully developed flow and heat transfer in semi-elliptical ducts, Int. J. Heat Fluid Flow 16 (1995) 145–152.
[6] K. Velusamy, V.K. Garg, Laminar mixed convection in vertical elliptic ducts, Int J. Heat Mass Transfer 39 (4) (1996) 745–752.

[7] E. Saatjian, R. Lam, J.P.B. Mota, Natural convection heat transfer in the annular region between porous confocal ellipses, Int. J. Numer. Meth. Fluids 31 (1999) 513–522.
[8] K. Velusamy, V.K. Garg, Entrance flow in elliptical ducts, Int. J. Numer. Meth. Fluids 17 (1993) 1079–1096.
[9] V.K. Garg, K. Velusamy, Developing flow in an elliptical duct, Int. J. Eng. Fluid Mech. 2 (2) (1989) 177–196.
[10] V. Javery, Analysis of laminar thermal entrance region of elliptical and rectangular channels with Kantorowich method, Wārme- und Stoffubertragung 9 (1976) 85–98.
[11] R.M. Abdel-Wahed, A.E. Attia, M.A. Hifni, Experiments on laminar flow and heat transfer in an elliptical duct, Int. J. Heat Mass Transfer 27 (12) (1984) 2397–2413.
[12] C.C.M. Rindt, J.J.M. Sillekens, A.A. Van Steenhoven, The influence of wall temperature on the development of heat transfer and secondary flow in a coiled heat exchanger, Int. Commun. Heat Mass Transfer 26 (2) (1999) 187–198.
[13] J. Schenk, B.S. Han, Heat transfer from laminar flow in ducts with elliptic cross section, Appl. Sci. Res. 17 (1966) 96–114.
[14] W.M. Kays, M.E. Crawford, Convective Heat and Mass Transfer, McGraw-Hill, 1993, p. 133 (Chapter 9).
[15] N. Conley, A. Lawal, A.S. Munjumdar, An assessment of the accuracy of numerical solutions to the Graetz problem, Int. Commun. Heat Mass Transfer 12 (1985) 219–222.